applied sciences

MDPI

Article

A Novel 3D Titanium Surface Produced by Selective Laser Sintering to Counteract *Streptococcus oralis* Biofilm Formation

Simonetta D'Ercole [1], Carlo Mangano [2], Luigina Cellini [3], Silvia Di Lodovico [3], Cigdem Atalayin Ozkaya [4], Giovanna Iezzi [1,5], Adriano Piattelli [6,7,8] and Morena Petrini [1,*]

1 Department of Medical, Oral and Biotechnological Science, University G. d'Annunzio of Chieti, Via dei Vestini 31, 66013 Chieti, Italy; simonetta.dercole@unich.it (S.D.); gio.iezzi@unich.it (G.I.)
2 Private Practice in Gravedonia, 22100 Como, Italy; camangan@gmail.com
3 Department of Pharmacy, University of Chieti, 66013 Chieti, Italy; l.cellini@unich.it (L.C.); silvia.dilodovico@unich.it (S.D.L.)
4 Department of Restorative Dentistry, School of Dentistry, Ege University, 35100 Izmir, Turkey; cigdem.atalayin@ege.edu.tr
5 Faculty of Medicine and Odontology, University of Valencia, 46004 Valencia, Spain
6 Faculty of Medicine and Odontology, Catholic University of San Antonio de Murcia (UCAM), Av. de los Jerónimos, 135, 30107 Murcia, Spain; adriano.piattelli@unich.it
7 Villa Serena Foundation for Research, Via Leonardo Petruzzi 42, 65013 Città Sant'Angelo, Italy
8 Casa di Cura Villa Serena del Dott. L. Petruzzi, Via Leonardo Petruzzi 42, 65013 Città Sant'Angelo, Italy
* Correspondence: morena.petrini@unich.it

Featured Application: This novel titanium surface, characterized by antiadhesive activity, could prevent the onset of peri-implantitis or medical device infections.

Abstract: The topography of implant surfaces influences the interaction relationship between material and bacteria. The aim of this work was to characterize a novel 3D titanium surface, produced using Selective Laser Sintering (SLS), and to compare the bacterial interaction with machined and double acid etching (DAE) discs. The surface was characterized by atomic force microscopy (AFM), scanning electron microscopy (SEM), and Energy Dispersive X-ray Spectrometry (EDX). The wettability was measured using the sessile method. The microbiological investigation consisted in the cultivation of a bacterial pioneer, *Streptococcus oralis*, on titanium surfaces, previously covered by human saliva in order to form the acquired pellicle. Then, colony forming units (CFUs), biofilm biomass quantification, analyses of viable and dead cells, and SEM observation were determined after 24 h of *S. oralis* biofilm formation on the different discs. A significantly higher nano-roughness with respect to the other two groups characterized the novel 3D surface, but the wettability was similar to that of machined samples. The microbiological assays demonstrated that the 3D discs reported significantly lower values of CFUs and biofilm biomass with respect to machined surfaces; however, no significant differences were found with the DAE surfaces. The live/dead staining confirmed the lower percentage of living cells on DAE and 3D surfaces compared with the machined. This novel 3D surface produced by SLS presented a high antiadhesive and antibiofilm activity.

Keywords: 3D printing; selective laser sintering; titanium; bacteria; biofilm

Citation: D'Ercole, S.; Mangano, C.; Cellini, L.; Di Lodovico, S.; Atalayin Ozkaya, C.; Iezzi, G.; Piattelli, A.; Petrini, M. A Novel 3D Titanium Surface Produced by Selective Laser Sintering to Counteract *Streptococcus oralis* Biofilm Formation. *Appl. Sci.* **2021**, *11*, 11915. https://doi.org/10.3390/app112411915

Academic Editor: Oleh Andrukhov

Received: 25 October 2021
Accepted: 8 December 2021
Published: 15 December 2021

1. Introduction

Three-dimensional printing is an additive manufacturing technology (AM) that represents an alternative method of production with respect to traditional casting and subtractive methods for producing tridimensional tools. This novel technology permits freeform fabrication, so in the biomedical field, custom-made tools can be fabricated, starting from patients records, such as X-rays or CT-scans [1,2]. AM can be applied in the production of bone substitutes and metallic meshes for guided bone regeneration, facilitating adaptation

and immobilization of the tool in the bony defect, reducing surgical times and post-surgical sequelae, and increasing the success rate of surgery [3–5].

A further advantage of AM is the possibility to plan the production of infinite complex geometries characterized by different porosities in order to mimic natural tissues [6]. With respect to the traditional process of fabrication, 3D printing represents an economic alternative that minimizes the amount of material wasted, reduces the number of steps needed in production, and influences the technician's ability to produce high-quality products [3]. An interesting review by Ni et al. described the different technologies adopted by recent 3D printers for the production of metallic biomedical devices [1]. In power bed fusion techniques, a high energetic beam, such as LASER, can be used to sinter (selective laser sintering, SLS) or melt (selective laser melting, SLM) different layers of metal powder deposited consecutively, based on a computer-aided design (CAD) project. The metal powder is delivered by a nozzle via the laser direct metal deposition (LDMD), so this technique permits a user to use different mixtures of metal powder to produce structures with different pores and gradients of metals, with the possibility to fabricate a large number of parts, and with a precision limit that is above 1 mm [7,8]. In selective electron beam melting (SEBM), the laser is substituted by a high-energy electron beam, with high efficiency of production and smaller deformation [9,10].

The metallic powder can also be trapped in a binder, which could be a plastic such as in atomic diffusion additive manufacturing (ADAM), or in a liquid ink, such as in the nanoparticle jetting (NPJ): in both techniques, the binder evaporates during the heating of the structure [11,12]. Laser-induced forward transfer (LIFT) involves applying a pulsed laser beam to a thin metallic film that melts and is deposited as droplets, which after cooling, solidify [13].

On the contrary, in inkjet 3D binder jetting, a water jet is layered on a metallic bed, forming a 3D structure that is sintered on a furnace.

Three-dimensional printing permits a user to modulate many parameters during the process of manufacturing, such as the energy power source, the temperature reached during manufacturing processes, the metallic powder adopted (composition and morphology), and the thickness of the deposited layers. It is important to highlight that the manufacturing method is able to affect the final product, especially in the chemical composition, the porous microstructure, and the mechanical properties.

Another important point to consider is the bacterial interaction with this novel surface: recent literature has highlighted the importance of surface topography in the contrast or in the establishment of a mature biofilm, which could protect or predispose to peri-implantitis [14–16]. Peri-implantitis is associated with complex microbiota profiles and the process of biofilm formation on the implant surface is comparable with biofilm formation on natural teeth. The species *Streptococcus oralis* and *Streptococcus sanguinis* followed by *Neisseria pharyngis* and *Gemella haemolysans* are considered the first colonizers of the implant surface. Changes in the biofilm composition of *Streptococci* species are observed between the fourth and eighth hours of biofilm formation. The first colonizers correlate positively with each other and influence the colonization of bacteria of orange and red complexes during the development of peri-implantitis [17].

The surface structure and hydrophobicity influence the capability of the bacteria to colonize and to form biofilm. In particular, the presence of concave features such as valleys or depression enhance the bacterial colonization [18]. McGaffey et al. demonstrated that manual polishing of 3D-printed surfaces reduced biofilm formation, with preparation-specific relationships between surface roughness and biofilm growth suggesting that metallic implants produced by laser powder bed fusion should be polished [18].

The primary objective of this study is to characterize the chemical composition, and the nano- and micro-topographies of a novel 3D surface produced in Ti6 Al4V through the SLS. The secondary objective is to evaluate the *Streptococcus oralis* interaction with this novel surface in comparison with two traditionally titanium surfaces already used in dental implantology: the machined and the titanium double acid etching (DAE).

The third objective is to correlate the topographical features of the surfaces with the microbiological results in order to identify those parameters that are more influential for bacterial growth.

2. Materials and Methods

The present study was conducted in accordance with the appropriate EQUATOR guidelines, the Standards for Reporting Qualitative Research SRQR [19].

Before incubation, all discs were immersed 60 min in 75% ethanol, left to dry, and sterilized by exposing the upper and lower surfaces to UV light for 30 min. A total of 108 discs were analyzed, compared in this study, and divided in three different groups, characterized by different chemical compositions, superficial topographies, and manufacturing processes:

- MACHINED: Titanium (Ti) IV grade (ASTM F67, Resista, Omegna (VB), Italy.
- DAE (double acid etched): Titanium IV grade (ASTM F67) double acid etched: the first with a solution containing fluorhydric acid and the second with nitric acid (Resista, Omegna (VB), Italy).
- 3D: Porous titanium alloy TiAl6V4 disks were designed with an open cell form (interconnected pores) through SolidWorks® 12.0 (SolidWorks Corp., Concord, MA, USA) and produced by a selective laser melting (SLM) machine (RenAM 500Q—Renishaw, Wotton-under-Edge, United Kingdom). The building parameters were a laser power of 200 W with a speed of 0.9 m/s, as previously described [20].

After that, the 3D discs underwent a post-processing treatment to eliminate the titanium spherical non-adherent particles from the surfaces.

The discs were sonicated 5 min in distilled water at 25 °C, immersed in NaOH (20 g/L) and hydrogen peroxide (20 g/L) at 80 °C for 30 min, and further sonicated 5 min in distilled water. Then, the discs were subjected to further cleaning in a mixture of 50% oxalic acid and 50% maleic acid at 80 °C for 45 min and washed for 5 min in distilled water in a sonic bath, as previously reported [20,21].

2.1. Scanning Electron Microscopy (SEM) and Energy Dispersive X-ray Spectrometry (EDX)

A Phenom ProX scanning electron microscope (Phenom-World BV, Eindhoven, the Netherlands) was utilized with the Element Identification (EID) package (Phenom ProSuite Software, Phenom-World B.V., Eindhoven, The Netherlands). This equipment allowed us to analyze the discs' micro topography and to perform the EDX analysis for the chemical composition of the upper layer of the samples, as previously described [15].

ImageJ Software 1.52q (National Institute of Health (NIH), Bethesda, MD, USA) with the plugin SurfCharJ was used to 3D reconstruct five different sections of size 200 µm × 200 µm for each group and then to calculate the average microroughness parameters: Root mean square deviation (MRq), Arithmetical mean roughness deviation (MRa), and Surface Area (MSa) [22].

2.2. Atomic Force Microscopy (AFM)

A Bruker AFM (Billerica, MA, USA) with the ScanAsyst technique was used to characterize the samples, as previously described [14,15]. With the help of the Nanoscope software (Bruker, MA, USA), it was possible to analyze images, the 3D reconstruction and the calculation of the following height parameters: surface roughness (Ra), root mean squared surface roughness (Rq), maximum surface roughness (Rmax), root-mean-square of the surface slope (Sdq), and developed interfacial area ratio (Sdr).

2.3. Measurement of Wettability of the Discs

The water contact angles (WCA) of the samples were determined using the sessile drop method. The water contact angle was measured using ImageJ 1.52q for Mac OS X (Apple Inc., Cupertino, CA, USA), as previously described [14,15].

2.4. Microbiological Analysis

The local Ethical Committee (approval code SALI, N. 19 of the 10 September 2020 Ethics Committee of University "G. d'Annunzio", Chieti-Pescara, Italy) approved the use of human saliva for this in vitro study. Four healthy volunteers donated their saliva, which was sampled using the spitting method. The inclusion criteria were age >18 years old and absence of chronic systemic diseases. The exclusion criteria were antibiotic treatments within 1 month prior to the study [23]. The saliva was gently agitated for 10 min, centrifugated for 1 h at 16,000 rounds at 4 °C, sterilized through a 0.2 µm filter, and frozen at −20 °C [24].

The immersion of the discs for 2 h in saliva at 37 °C permitted the formation of the acquired pellicle in order to mimic the clinical conditions [14,15,24].

2.5. Preparation of Bacterial Suspension

The frozen (−80 °C) *Streptococcus oralis* CH 05 previously characterized [25] was recovered in Brain Heart Infusion broth (BHI, Oxoid, Milan, Italy), diluted, and standardized at Optical Density ($OD_{600\ nm}$ 0.125 ≅ 9 × 10^6 CFU/mL) as previously described [14,15].

Then, 200 µL of the standardized broth culture was inoculated on the discs, previously coated with saliva, and left to incubate at 37 °C for 24 h under anaerobic condition [14,15].

Before the quantification of the colony forming units (CFUs), the biomass, the SEM, and live/dead observation, the discs were rinsed with PBS three times to remove the free bacteria.

Non-inoculated titanium discs were used as negative controls.

2.6. Determination of Colony-Forming Units (CFUs)

The discs covered by bacteria were put on sterile test tubes with 1 mL PBS, ultrasonicated for 4 min with a 4 kHz ultrasonic cleaning water bath (Euronda, Vicenza, Italy), and vortexed for 2 min to detach the bacteria adherent to the specimen surface [14,15].

The mixture was observed in a microscope through live/dead staining, as described in the next section in order to confirm that the suspension was composed by single microbial cells.

Then, the CFU/mL determination for each disc were performed by spreading the 10-fold dilutions on Tryptic Soy Agar (TSA). The plates were incubated at 37 °C per 24 h.

2.7. Biofilm Biomass Assay

Biofilm biomass adherent to the specimen surface was assessed by Crystal Violet (0.1%) (Sigma-Aldrich, Milan, Italy) staining for 1 min, washing with PBS, and 10 min elution with ethanol in order to proceed for absorbance reading (AU) at 570 nm with a microplate reader (SAFAS, Munich, state abbr. (if has), Germany). The AU is proportional to the biomass.

2.8. Viability Test

The discs with adherent bacteria cells were stained using the BacLight live/dead Viability Kit (Molecular Probes, Invitrogen-Thermo Fisher Scientific, Milan, Italy) and analyzed by the fluorescent microscope Leica 4000 DM microscopy (Leica Microsystems, Milan, Italy). It permitted us to observe the SYTO 9 (green fluorescence) that stained the viable cells at 500 nm and, on the contrary, (red fluorescence) those with impaired membrane activity that were stained with propidium iodide at 635 nm.

The evaluation was performed by three blinded microbiologists by examining at least 10 visual fields each, in a random way.

2.9. Statistical Analysis

Each analysis was performed in triplicate, and the mean values (± standard deviation) were considered for the statistical analysis. Statistical analysis was performed using SPSS for Windows version 21 (IBM SPSS Inc., Chicago, IL, USA), and analysis of variance

(ANOVA) and the Fisher's Least Significant Difference (LSD) test were used to compare the parameters analyzed in the study for intra- and inter-group analysis. The Pearson analysis was used to evaluate the presence of significant correlations between the parameters analyzed in this study.

p-values less than 0.05 were considered significant.

3. Results

The microscopical aspect of the novel disc presented with a very high porosity and a uniform 3D framework at the SEM observation (Figure 1A,B). At 480× of magnification, the surface appeared as a net of melted metal uniformly interconnected by craters, filled by sintered metallic particles (Figure 1C). The porous aspect of the material was even more evident from the 3D reconstruction (Figure 1D).

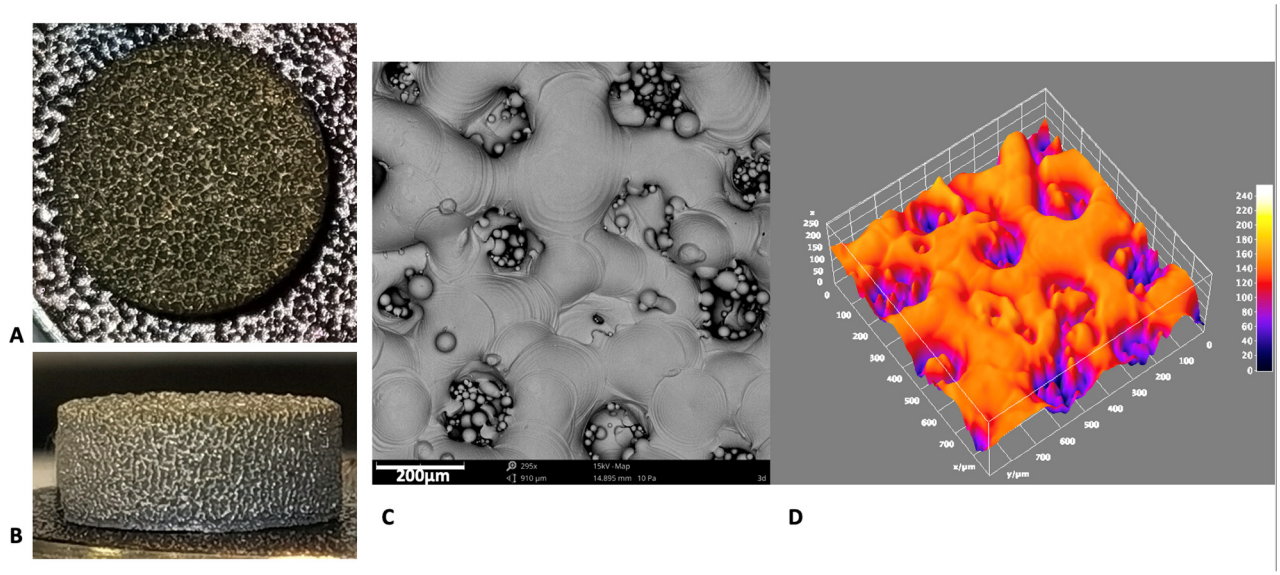

Figure 1. Photograph of the novel 3D surface, upper (**A**) and lateral (**B**) views. (**C**) SEM image at 480× magnification of the novel 3D surface and (**D**) the respective 3D reconstruction.

Analyzing and comparing the three surfaces at higher magnification (1200×) and in the 3D reconstruction, the greater difference in superficial topographies between the three groups was evident: the machined one (Figure 2A,D) had a regular superficial structural appearance, with characteristic circumferential and parallel lines; DAE (Figure 2B,E) had a very irregular surface, characterized by a high porosity with holes of different shapes and sizes. The 3D discs (Figure 2C,F) appeared in about the 50% of the image, as a uniform rough surface, that in the other 50% was characterized by the presence of a high crater, containing semi-molded metallic powders. The average values ± standard deviation of the microroughness parameters calculated are shown on Table 1. The DAE samples were characterized by the higher micro-roughness, with statistically significant differences with respect to the machined one but not with respect to the 3D one (Table 1). The surfaces showed statistically significant differences between all groups, with DAE characterized by the highest values, followed by the machined and 3D ones.

The EDX analysis (Figure 3), performed at 5kV, showed that the upper layer of the 3D samples was characterized by the presence of Al and Al_2O_3. Consequently, a significantly lower concentration of TiO_2 was found with respect to the machined and DAE samples ($p < 0.001$). The weight Ti concentration (%) was significantly lower on the 3D samples with respect to the machined ($p = 0.007$) and DAE ($p = 0.014$) discs.

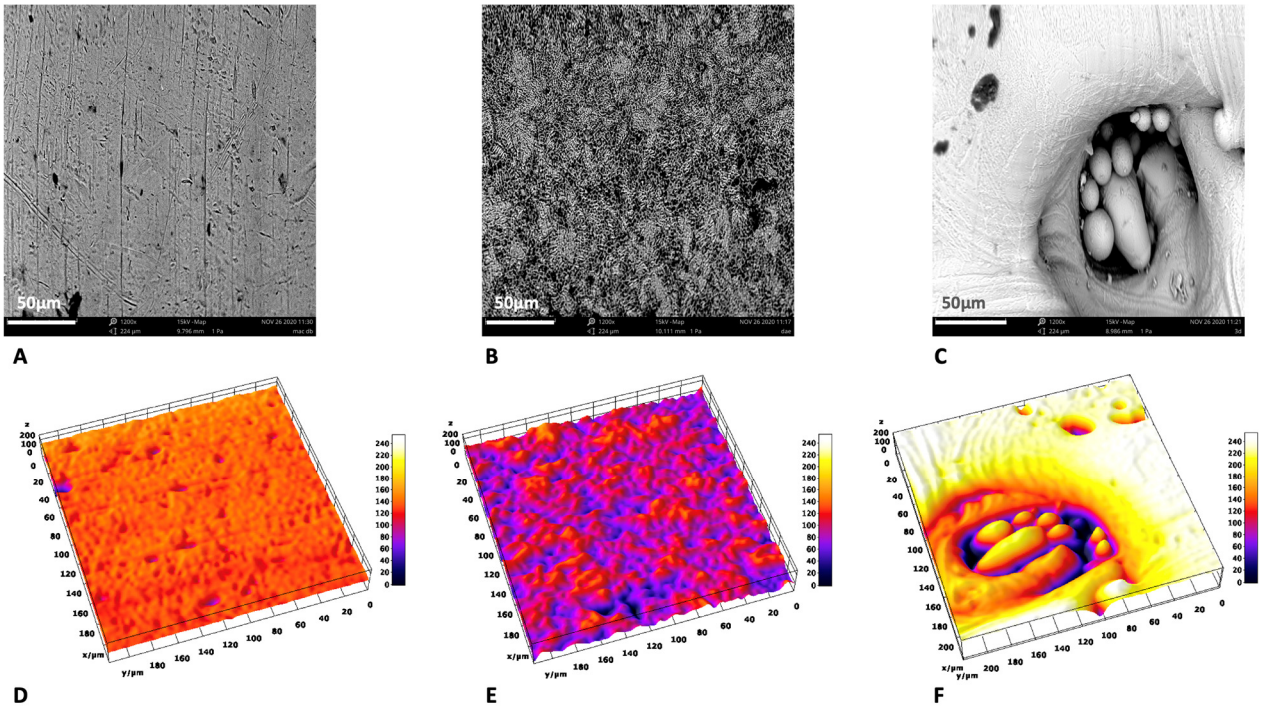

Figure 2. Comparison of SEM images at 1200× with the respective 3D reconstruction: machined (**A**,**D**), DAE (**B**,**E**), and 3D (**C**,**F**).

Table 1. The Pearson correlations calculated for CFUs and biomass vs. the other parameters investigated in this study.

			BIOMASS	CFUs				BIOMASS	CFUs
EDX analysis	Atomic TI	Pearson's Correlation	0.671 *	0.828 **	**AFM height parameters**	Ra	Pearson's Correlation	−0.793 *	−0.764 *
		Sig. (2-code)	0.048	0.006			Sig. (2-code)	0.011	0.017
	atomic O	Pearson's Correlation	−0.26	−0.694 *		Rq	Pearson's Correlation	−0.755 *	−0.824 **
		Sig. (2-code)	0.499	0.038			Sig. (2-code)	0.019	0.006
	weight Ti	Pearson's Correlation	0.754 *	0.828 **		Rmax	Pearson's Correlation	−0.612	−0.867 **
		Sig. (2-code)	0.019	0.006			Sig. (2-code)	0.08	0.002
	weight O	Pearson's Correlation	−0.296	−0.705 *		Sdq	Pearson's Correlation	−0.706 *	−0.866 **
		Sig. (2-code)	0.44	0.034			Sig. (2-code)	0.033	0.003
	TiO2 Stoich.	Pearson's Correlation	0.894 **	0.705 *		Sdr	Pearson's Correlation	−0.765 *	−0.758 *
		Sig. (2-code)	0.001	0.034			Sig. (2-code)	0.016	0.018
	atomic Al	Pearson's Correlation	0.976	0.596	**Micro-roughness**	MRq	Pearson's Correlation	0.290	−0.440
		Sig. (2-code)	0.139	0.593			Sig. (2-code)	0.450	0.203
	weight Al	Pearson's Correlation	0.999 *	0.444		Mra	Pearson's Correlation	0.354	−0.400
		Sig. (2-code)	0.025	0.707			Sig. (2-code)	0.349	0.252
	Al2O3 Stoich.	Pearson's Correlation	0.999*	0.379		Msa	Pearson's Correlation	0.888 **	0.188
		Sig. (2-code)	0.02	0.753			Sig. (2-code)	0.001	0.602
Wettability	WCA	Pearson's Correlation	−0.710 *	0.11					
		Sig. (2-code)	0.032	0.777					

* p significant at ≤ 0.05. ** p significant at ≤ 0.01.

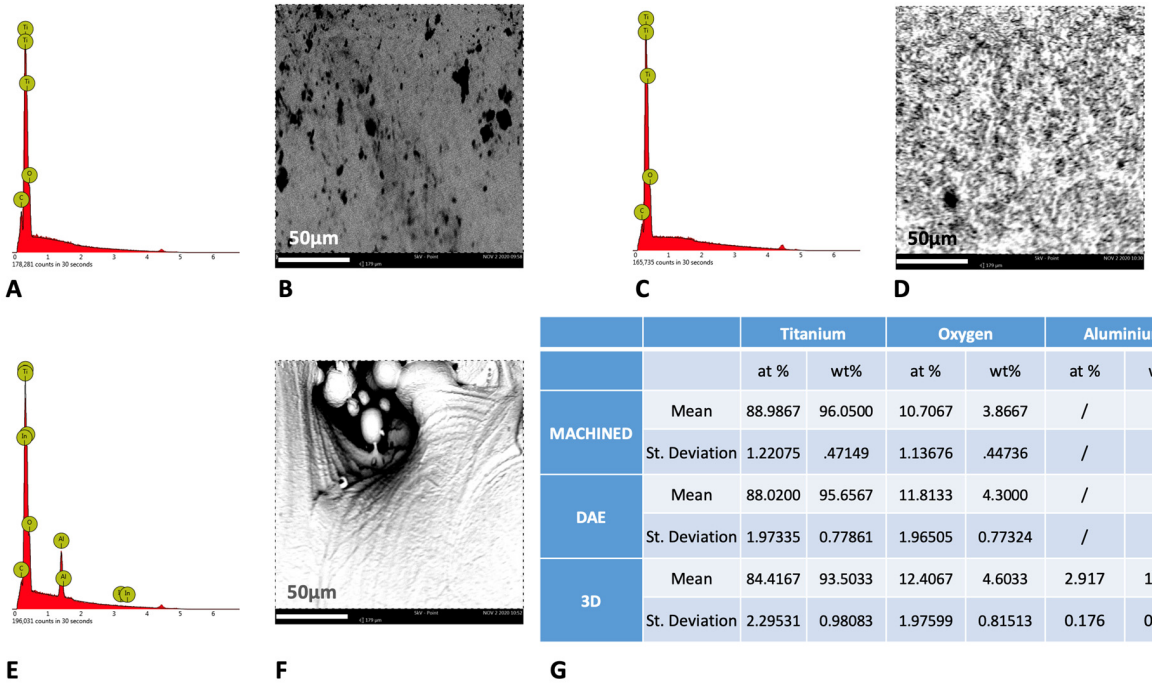

		Titanium		Oxygen		Aluminium		Stoich.	
		at %	wt%	at %	wt%	at %	wt%	TiO_2	Al_2O_3
MACHINED	Mean	88.9867	96.0500	10.7067	3.8667	/	/	99.9467	/
	St. Deviation	1.22075	.47149	1.13676	.44736	/	/	0.01528	/
DAE	Mean	88.0200	95.6567	11.8133	4.3000	/	/	99.9733	/
	St. Deviation	1.97335	0.77861	1.96505	0.77324	/	/	0.00577	/
3D	Mean	84.4167	93.5033	12.4067	4.6033	2.917	1.820	97.7967	2.157
	St. Deviation	2.29531	0.98083	1.97599	0.81513	0.176	0.135	0.20841	0.171

G

Figure 3. Spectra of energy dispersive X-ray spectrometry (EDS) analysis at 5 kV of machined (**A**), DAE (**C**), and 3D (**E**) titanium discs with the respective picture of the surfaces analyzed at 1200× (**B**,**D**,**F**). (**G**) The chemical composition (average values ± standard deviation) of the samples analyzed by EDS at 5 kV.

The observation at AFM demonstrated that the 3D showed a significant higher nano-roughness with respect to the other groups for all height parameters analyzed (Figure 4). The DAE and machined discs showed no significant differences, with the exception of the Sdq and Sdr values ($p = 0.020$).

The analysis of the wetting properties of the samples showed that the DAE samples' WCA was significantly lower with respect to the other two groups, $p < 0.001$ (Figure 5). On the contrary, the WCA of the machined (87.713° ± 1.732) and 3D discs (86.094° ± 1.535) showed no significant differences.

The microbiological analysis showed that *S. oralis* colonization was significantly lower on 3D discs, concerning the colony forming units from the biofilm biomass measurement (Figure 6). Regarding the CFUs, no significant differences were described for DAE and 3D discs, but for the biofilm biomass, it was significantly higher on double etched surfaces. The machined surface showed the higher levels of *S. oralis* CFUs.

The Pearson correlation between the parameters studied showed that CFUs were inversely correlated with the nano-roughness of the samples and with the chemical composition of the upper layers of the discs, in particular with the Oxygen and Aluminum percentages (Table 1). A direct correlation was found between the bacterial count and the Ti percentage.

The biofilm biomass was directly correlated with the percentage of Ti and aluminum in the upper layer of the samples and with the Surface Area (MSa) and inversely correlated with the nano-roughness.

The live/dead analysis (Figure 7) confirmed the *S. oralis* bacterial reduction on DAE and 3D surfaces with respect to machined and positive controls C+, which showed a higher percentage of live cells with respect to the other groups. The 3D sample was characterized by a 1:1 ratio between live and dead cells; on the contrary, the percentage of dead cells increased on DAE surfaces.

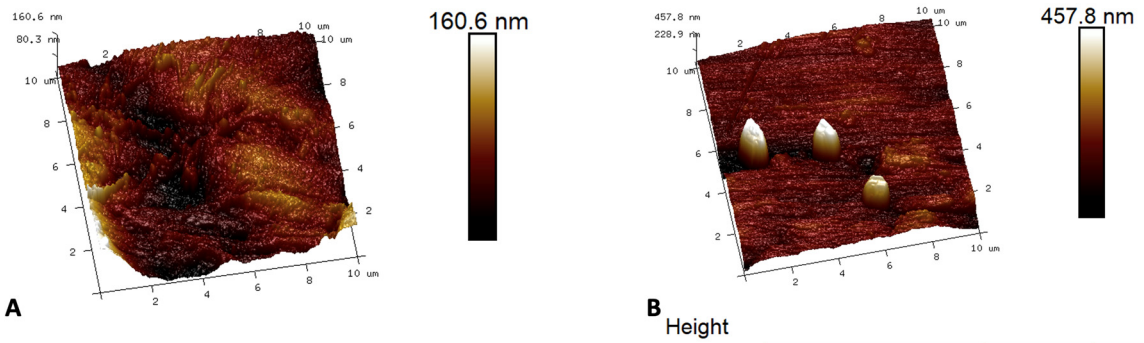

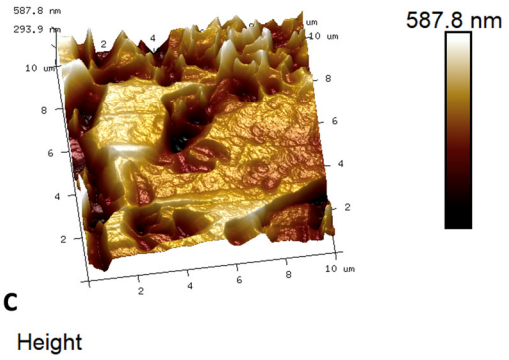

D

AFM ANALYSIS		AVERAGE VALUE	STANDARD DEVIATION	LSD analysis: 3D vs. :
Ra	MACHINED	21.033	5.948	$p = 0.001$*
	DAE	29.067	8.609	$p = 0.002$*
	3D	84.267	20.573	/
Rq	MACHINED	27.500	8.227	$p = 0.001$*
	DAE	44.533	13.661	$p = 0.003$*
	3D	107.900	23.478	/
Rmax	MACHINED	264.667	15.503	$p = 0.001$*
	DAE	515.000	123.984	$p = 0.016$
	3D	865.333	187.014	/
Sdq	MACHINED	7.677	1.426	$p < 0.001$**
	DAE	16.333	2.658	$p = 0.001$*
	3D	32.867	4.972	/
Sdr	MACHINED	0.910	0.318	$p = 0.001$*
	DAE	4.026	1.282	$p = 0.003$*
	3D	18.867	6.264	/

Figure 4. Three-dimensional reconstruction of AFM images of the different surfaces: machined (**A**), DAE (**B**), and 3D (**C**) with the relative table (**D**) of the average values (+/− standard deviation) of the surface nano-roughness parameters measured: surface roughness (Ra), root mean squared surface roughness (Rq), maximum surface roughness (Rmax), root-mean-square of the surface slope (Sdq), developed interfacial area ratio (Sdr), and the post hoc LSD analysis of intergroup comparison between nano-topographical parameters measured on AFM observations * p-value < 0.05. ** p-value < 0.001.

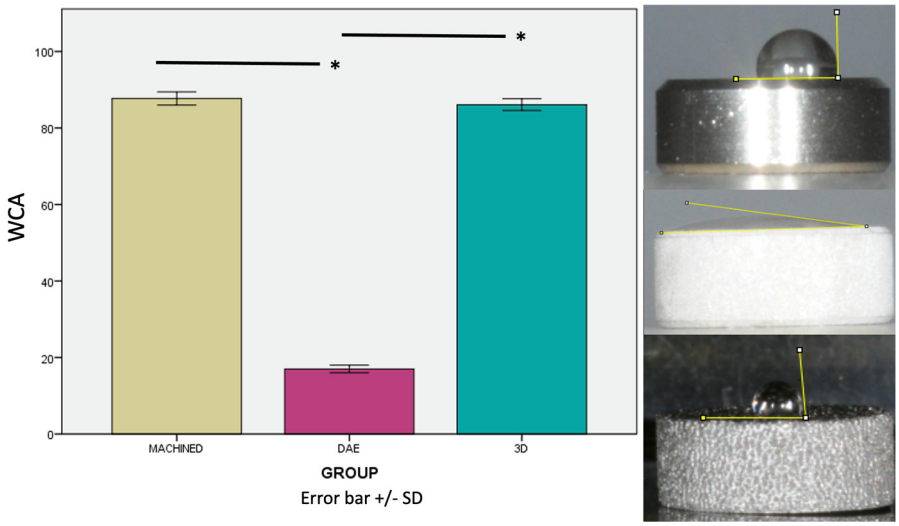

Figure 5. Photographs and relative graphics of water contact angles (WCA) measured with the sessile drop method. Error bars = +/− standard deviation. * p-value < 0.05.

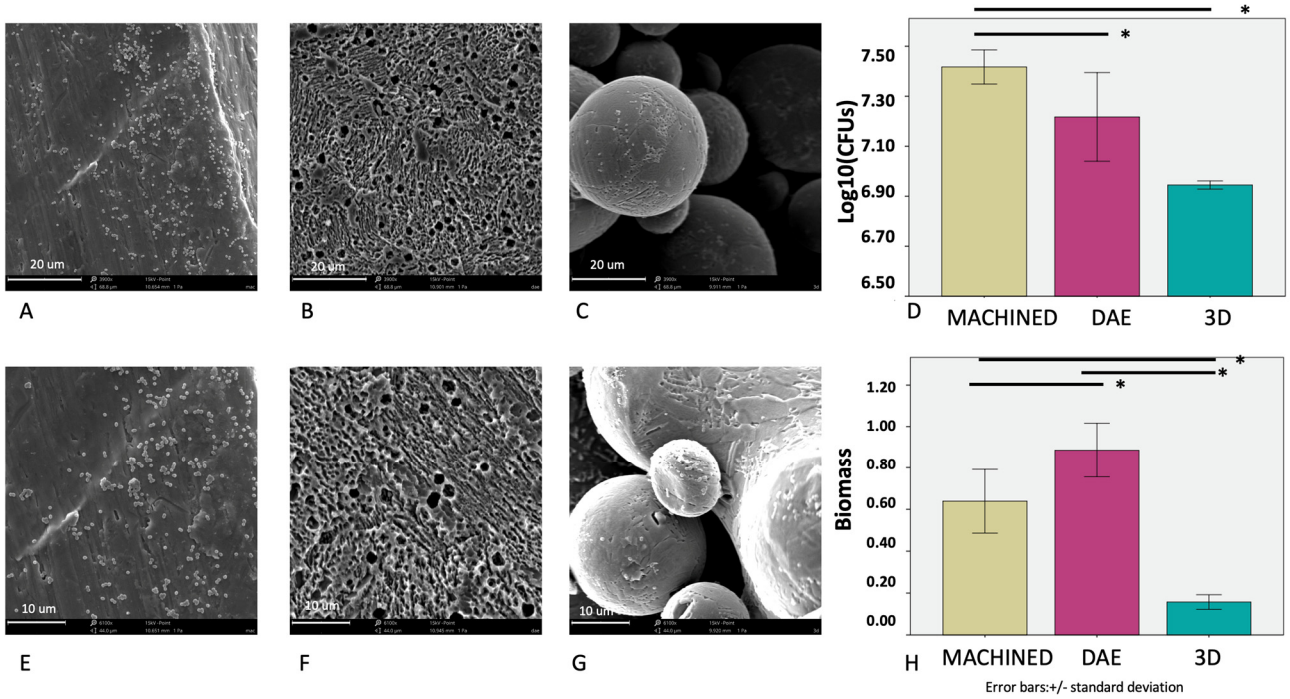

Figure 6. SEM observations of the different surfaces covered by the bacterial biofilm: machined (3900× **A**, 6100× **E**), DAE (3900× **B**, 6100× **F**), and 3D (3900× **C**, 6100× **G**). The average values of the colony forming units (log10)/mL (**D**) and biofilm mass formation (**H**) of *S. oralis* at 48 h (error bars = +/− standard deviation). * *p* significant at 0.05.

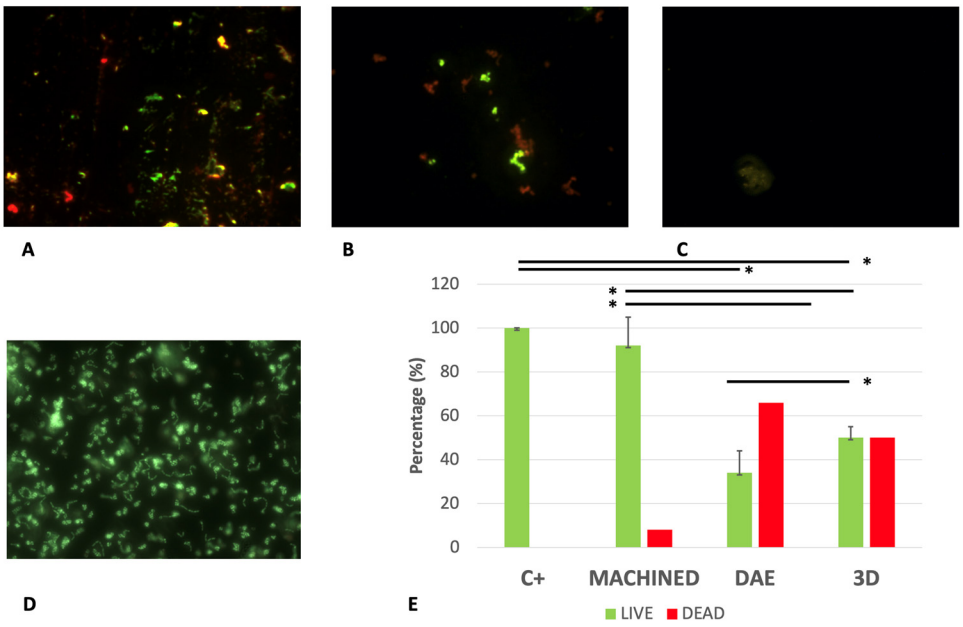

Figure 7. Representative images of live/dead staining of *Streptococcus oralis* biofilm growth on different titanium surfaces: machined (**A**), DAE (**B**), and 3D (**C**) samples and positive controls (**D**). Average percentage of viable (green) and dead (red) cells on different groups (**E**). Error bars = +/− standard deviation. * *p*-value < 0.01.

4. Discussion

The production of metallic implants and biomedical tools with the help of 3D printing has spread considerably in recent years. However, the main cause of failures, both early and late, of orthopedic prostheses, dental implants, and membranes for guided bone regeneration is bacterial colonization [26]. Current research in dentistry and biomedical

devices aims to find novel materials and technologies able to counteract the bacterial growth but at the same time to accelerate the healing of infected sites or to promote the bone osseointegration of dental implants and bone prosthesis [14,27,28].

The novel surfaces are manufactured and designed with a high porosity in order to increase interaction with cells, and to promote accelerated healing and osteointegration. The 3D sample was chosen from a group of other titanium ones, produced by SLM and tested on a previous study [21]. In particular, it showed not only biocompatibility but also the ability to increase the Dental Pulp Stem Cells (DPSCs) proliferation paralleled by the decrease in LDH released in a time-dependent manner [21]. The 3D surface showed a behavior resembling the inner structure of native bone, allowing cells to better adhere inside the specimen, with proteins related to cell adherence being highly expressed.

It also showed osteoconductive properties, with the profile of osteogenic markers being improved compared with titanium samples [21].

However, once that pioneer bacteria colonized a biomaterial, the procedure for bacterial removal could be very difficult, especially for the ability of the biofilm to protect bacteria against antibiotics, so novel treatments have been proposed and studied [28].

Consequently, the introduction of novel materials and surfaces that could contrast the adhesion of bacterial pioneers, such as *Streptococcus oralis*, could represent a real advancement for the prevention of this disease [14,15]. In this study, *S. oralis* was used because it is an early colonizer during the process of biofilm formation on implant surface and provides the basis for the subsequent colonization of facultative and obligate anaerobes.

The novel 3D surface, investigated in this study, had the advantages of being manufactured through SLM, so a tridimensional geometry was computer-projected in order to promote cellular interactions and osseointegration. This 3D surface showed very impressive results against *S. oralis*, especially when compared with machined discs. The 3D one was characterized by high nano-roughness and oxygen content in the upper layers and a good micro-roughness that presumably contributed in the reduction in bacterial CFUs, as previously found in the literature [14,15]. Indeed, as suggested by Lorenzetti et al., the presence of nano-roughness could act as a spacer between titanium and bacteria, which are characterized by a rigid structure [29]. Another difference between 3D discs and the other groups is the chemical composition; as shown in the EDX analysis, the 3D contained a certain percentage of aluminum because it was manufactured with a Ti6Al4V alloy contrary to the machined and DAE samples, which were in pure Ti. However, there is evidence that commercial pure Ti or Ti-6Al-4V alloy does not demonstrate antimicrobial properties [30]. Additionally, DAE surfaces were characterized by a good antibacterial activity, as confirmed by the low CFUs, in accordance with previous studies, but the biofilm biomass was significantly higher with respect to other groups [14,15]. However, the live/dead analysis also confirmed that DAE and 3D discs were characterized by the higher presence of dead cells with respect to machined and positive controls. It is known that bacteria are able to modify their cell size, shape, and other features, such as the growing rate, under the influence of the environment [31]. Additionally, the biofilm production is a consequence of the environment: the high micro-surface area (Msa), which characterized DAE surfaces, was correlated with a higher biofilm biomass production. Indeed, a high surface area potentially increases the bacteria adherence to the surface and biofilm formation that depends first upon the adhesion of cells to a surface [32]. This study should be considered as preliminary observation because it is based on a bacterial mono-specie model. However, *Streptococcus oralis* is a pioneer and consequently is one of the bacterial species able to interact with new surfaces and with the acquired pellicle, permitting the establishment of a polymicrobial mature biofilm.

The clinical relevance of these results are extremely important because this novel 3D titanium surface could represent a potential solution against biomaterial association infection and a valid option to reduce the bacterial colonization of implants and the consequent onset of peri-implantitis [33].

5. Conclusions

This novel 3D surface, produced by SLS, presented significant antibacterial activity and a good antibiofilm activity. The superficial features that influence bacterial colonization seem to be nano-roughness, the presence of superficial oxygen, and the micro-surface area.

Author Contributions: Conceptualization, S.D., S.D.L., M.P., and C.M.; methodology, S.D.L. and G.I.; software, C.M.; validation, S.D., M.P., A.P., and L.C.; formal analysis, M.P., C.A.O., C.M., and G.I.; investigation, S.D., S.D.L., and M.P.; resources, A.P., G.I., and L.C.; data curation, M.P. and S.D.; writing—original draft preparation, S.D. and M.P.; writing—review and editing, A.P., G.I., C.A.O., and L.C.; visualization, L.C.; supervision, A.P. and C.M.; project administration, S.D., S.D.L., and M.P.; funding acquisition, A.P., L.C., and S.D. All authors have read and agreed to the published version of the manuscript.

Funding: This research was funded by FAR Grants, 2021, S. D'Ercole, L. Cellini, M. Petrini.

Institutional Review Board Statement: The study was conducted according to the guidelines of the Declaration of Helsinki, and the use of human saliva was approved by the Ethical Committee of the University G. d'Annunzio of Chieti-Pescara, Italy (N. 19, 10 September 2020).

Informed Consent Statement: Informed consent was obtained from all subjects involved in the study.

Acknowledgments: Authors would like to thanks Serena Pilato, for the AFM. images.

Conflicts of Interest: The authors declare no conflict of interest.

References

1. Ni, J.; Ling, H.; Zhang, S.; Wang, Z.; Peng, Z.; Benyshek, C.; Zan, R.; Miri, A.K.; Li, Z.; Zhang, X.; et al. Three-dimensional printing of metals for biomedical applications. *Mater. Today Bio* **2019**, *3*, 100024. [CrossRef]
2. Revilla-León, M.; Sadeghpour, M.; Özcan, M. A Review of the Applications of Additive Manufacturing Technologies Used to Fabricate Metals in Implant Dentistry. *J. Prosthodont.* **2020**, *29*, 579–593. [CrossRef] [PubMed]
3. Kim, H.D.; Amirthalingam, S.; Kim, S.L.; Lee, S.S.; Rangasamy, J.; Hwang, N.S. Biomimetic Materials and Fabrication Approaches for Bone Tissue Engineering. *Adv. Healthc. Mater.* **2017**, *6*, 1700612. [CrossRef]
4. Zhang, L.; Yang, G.; Johnson, B.N.; Jia, X. Three-dimensional (3D) printed scaffold and material selection for bone repair. *Acta Biomater.* **2019**, *84*, 16–33. [CrossRef]
5. Wang, F.; Zhu, J.; Peng, X.; Su, J. The application of 3D printed surgical guides in resection and reconstruction of malignant bone tumor. *Oncol. Lett.* **2017**, *14*, 4581–4584. [CrossRef] [PubMed]
6. Jing, Z.; Zhang, T.; Xiu, P.; Cai, H.; Wei, Q.; Fan, D.; Lin, X.; Song, C.; Liu, Z. Functionalization of 3D-printed titanium alloy orthopedic implants: A literature review. *Biomed. Mater.* **2020**, *15*, 052003. [CrossRef]
7. Dinda, G.P.; Song, L.; Mazumder, J. Fabrication of Ti-6Al-4V Scaffolds by Direct Metal Deposition. *Metall. Mater. Trans. A* **2008**, *39*, 2914–2922. [CrossRef]
8. Ahsan, M.N.; Paul, C.P.; Kukreja, L.M.; Pinkerton, A.J. Porous structures fabrication by continuous and pulsed laser metal deposition for biomedical applications; Modelling and experimental investigation. *J. Mater. Process. Technol.* **2011**, *211*, 602–609. [CrossRef]
9. Heinl, P.; Rottmair, A.; Körner, C.; Singer, R.F. Cellular titanium by selective electron beam melting. *Adv. Eng. Mater.* **2007**, *9*, 360–364. [CrossRef]
10. Guo, N.; Leu, M.C. Additive manufacturing: Technology, applications and research needs. *Front. Mech. Eng.* **2013**, *8*, 215–243. [CrossRef]
11. Galati, M.; Minetola, P. Analysis of Density, Roughness, and Accuracy of the Atomic Diffusion Additive Manufacturing (ADAM) Process for Metal Parts. *Materials* **2019**, *12*, 4122. [CrossRef] [PubMed]
12. Gao, Y.; Shin, Y.K.; Martinez, D.; Manogharan, G.; van Duin, A.C.T. A ReaxFF molecular dynamics study of molecular-level interactions during binder jetting 3D-printing. *Phys. Chem. Chem. Phys.* **2019**, *21*, 21517–21529. [CrossRef]
13. Breckenfeld, E.; Kim, H.; Auyeung, R.C.Y.; Piqué, A. Laser-induced Forward Transfer of Ag Nanopaste. *J. Vis. Exp.* **2016**, e53728. [CrossRef] [PubMed]
14. D'Ercole, S.; Cellini, L.; Pilato, S.; Di Lodovico, S.; Iezzi, G.; Piattelli, A.; Petrini, M. Material characterization and *Streptococcus oralis* adhesion on Polyetheretherketone (PEEK) and titanium surfaces used in implantology. *J. Mater. Sci. Mater. Med.* **2020**, *31*, 84. [CrossRef]
15. Petrini, M.; Giuliani, A.; Di Campli, E.; Di Lodovico, S.; Iezzi, G.; Piattelli, A.; D'Ercole, S. The Bacterial Anti-Adhesive Activity of Double-Etched Titanium (DAE) as a Dental Implant Surface. *Int. J. Mol. Sci.* **2020**, *21*, 8315. [CrossRef]
16. Pokrowiecki, R.; Mielczarek, A.; Zaręba, T.; Tyski, S. Oral microbiome and peri-implant diseases: Where are we now? *Ther. Clin. Risk Manag.* **2017**, *13*, 1529–1542. [CrossRef] [PubMed]

17. Hall, D.C., Jr.; Palmer, P.; Ji, H.F.; Ehrlich, G.D.; Król, J.E. Bacterial Biofilm Growth on 3D-Printed Materials. *Front. Microbiol.* **2021**, *12*, 646303. [CrossRef]
18. McGaffey, M.; Zur Linden, A.; Bachynski, N.; Oblak, M.; James, F.; Weese, J.S. Manual polishing of 3D printed metals produced by laser powder bed fusion reduces biofilm formation. *PLoS ONE* **2019**, *14*, e0212995. [CrossRef] [PubMed]
19. O'Brien, B.C.; Harris, I.B.; Beckman, T.J.; Reed, D.A.; Cook, D.A. Standards for reporting qualitative research: A synthesis of recommendations. *Acad. Med.* **2014**, *89*, 1245–1251. [CrossRef]
20. Gallorini, M.; Zara, S.; Ricci, A.; Mangano, F.G.; Cataldi, A.; Mangano, C. The Open Cell Form of 3D-Printed Titanium Improves Osteconductive Properties and Adhesion Behavior of Dental Pulp Stem Cells. *Materials* **2021**, *14*, 5308. [CrossRef]
21. Zhang, Y. Electropolishing Mechanism of Ti-6Al-4V Alloy Fabricated by Selective Laser Melting. *Int. J. Electrochem. Sci.* **2018**, *13*, 4792–4807. [CrossRef]
22. Martinez, M.A.F.; de Balderrama, Í.F.; Karam, P.S.B.H.; de Oliveira, R.C.; de Oliveira, F.A.; Grandini, C.R.; Vicente, F.B.; Stavropoulos, A.; Zangrando, M.S.R.; Sant'Ana, A.C.P. Surface roughness of titanium disks influences the adhesion, proliferation and differentiation of osteogenic properties derived from human. *Int. J. Implant Dent.* **2020**, *6*, 46. [CrossRef] [PubMed]
23. Petrini, M.; Costacurta, M.; Ferrante, M.; Trentini, P.; Docimo, R.; Spoto, G. Association between the organoleptic scores, oral condition and salivary β-galactosidases in children affected by halitosis. *Int. J. Dent. Hyg.* **2014**, *12*, 213–218. [CrossRef]
24. D'Ercole, S.; Di Lodovico, S.; Iezzi, G.; Pierfelice, T.V.; D'Amico, E.; Cipollina, A.; Piattelli, A.; Cellini, L.; Petrini, M. Complex Electromagnetic Fields Reduce *Candida albicans* Planktonic Growth and Its Adhesion to Titanium Surfaces. *Biomedicines* **2021**, *9*, 1261. [CrossRef] [PubMed]
25. D'Ercole, S.; Di Giulio, M.; Grande, R.; Di Campli, E.; Di Bartolomeo, S.; Piccolomini, R.; Cellini, L. Effect of 2-hydroxyethyl methacrylate on *Streptococcus* spp. biofilms. *Lett. Appl. Microbiol.* **2011**, *52*, 193–200. [CrossRef]
26. Sridhar, S.; Wang, F.; Wilson, T.G.; Palmer, K.; Valderrama, P.; Rodrigues, D.C. The role of bacterial biofilm and mechanical forces in modulating dental implant failures. *J. Mech. Behav. Biomed. Mater.* **2019**, *92*, 118–127. [CrossRef]
27. Graziani, F.; Gennai, S.; Petrini, M.; Bettini, L.; Tonetti, M. Enamel matrix derivative stabilizes blood clot and improves clinical healing in deep pockets after flapless periodontal therapy: A Randomized Clinical Trial. *J. Clin. Periodontol.* **2019**, *46*, 231–240. [CrossRef]
28. Radunović, M.; Petrini, M.; Vlajic, T.; Iezzi, G.; Di Lodovico, S.; Piattelli, A.; D'Ercole, S. Effects of a novel gel containing 5-aminolevulinic acid and red LED against bacteria involved in peri-implantitis and other oral infections. *J. Photochem. Photobiol. B Biol.* **2020**, *205*, 111826. [CrossRef]
29. Lorenzetti, M.; Dogša, I.; Stošicki, T.; Stopar, D.; Kalin, M.; Kobe, S.; Novak, S. The influence of surface modification on bacterial adhesion to titanium-based substrates. *ACS Appl. Mater. Interfaces* **2015**, *7*, 1644–1651. [CrossRef]
30. Chen, M.; Li, H.; Wang, X.; Qin, G.; Zhang, E. Improvement in antibacterial properties and cytocompatibility of titanium by fluorine and oxygen dual plasma-based surface modification. *Appl. Surf. Sci.* **2019**, *463*, 261–274. [CrossRef]
31. Harris, L.K.; Theriot, J.A. Surface Area to Volume Ratio: A Natural Variable for Bacterial Morphogenesis. *Trends Microbiol.* **2018**, *26*, 815–832. [CrossRef] [PubMed]
32. Nobbs, A.H.; Lamont, R.J.; Jenkinson, H.F. Streptococcus Adherence and Colonization. *Microbiol. Mol. Biol. Rev.* **2009**, *73*, 407–450. [CrossRef] [PubMed]
33. Riool, M.; de Boer, L.; Jaspers, V.; van der Loos, C.M.; van Wamel, W.J.B.; Wu, G.; Kwakman, P.H.S.; Zaat, S.A.J. *Staphylococcus epidermidis* originating from titanium implants infects surrounding tissue and immune cells. *Acta Biomater.* **2014**, *10*, 5202–5212. [CrossRef] [PubMed]